Microestructural and ferroelectric analyses of $Pb_{1-3x/2}La_x(Zr_{0.54}Ti_{0.46})_{1-5y/4}Nb_yO_3$ soft ceramics.

Análisis microestructural y ferroeléctrico de cerámicas suaves de $Pb_{1-3x/2}La_x(Zr_{0.54}Ti_{0.46})_{1-5y/4}Nb_yO_3$

M.D. Durruthy-Rodríguez[1], M. Hernández-García[1], J.M. Yañez-Limón[2], D. Rivero Ramírez[3], F.J. Espinoza Beltrán[2]

[1]UNEV- Santo Domingo, Paseo de los Periodistas 54, Miraflores, CP 10230, Santo Domingo D.N., República Dominicana. mddurruthy@gmail.com
[2]CINVESTAV-Unidad Querétaro, IPN, Libramiento Norponiente 2000, Fraccionamiento Real de Juriquilla, CP 76230, Querétaro, Qro, México. jmyanez@cinvestav.mx
[3]Facultad de Ciencias y Tecnologías Nucleares, Quinta de los Molinos. Ave Carlos III y Luaces, CP 10600, La Habana, Cuba. doris@instec.cu

Abstract: Microstructural and ferroelectric analyses were carried out on $Pb_{1-3x/2}La_x(Zr_{0.54}Ti_{0.46})_{1-5y/4}Nb_yO_3$ ceramics, x = y = 0.004, 0.006, 0.008 and 0.01 mol%. Using Piezoresponse Force Microscopy (PFM) and piezoelectric Hysteresis Loop (HL), ferroelectric behavior, and ferroelectric domain sizes were determined. Grain size (as determinate by SEM) and ferroelectric domain area decrease with the increase of dopant concentration from 3 μm to 1 μm and from 0.56 μm^2 to 0.32 μm^2, respectively. The maximum remnant polarization was obtained for $Pb_{0.985}La_{0.01}(Zr_{0.54}Ti_{0.46})_{0.9875}Nb_{0.01}O_3$, showing that samples polarize easier with higher La^{3+} and Nb^{5+} dopant concentration. The coercive field does not show significant differences as the La and Nb content is varied. Grains tend to be single crystals as the La^{3+} and Nb^{5+} dopant concentration is increased.

Keywords: Ferroelectric materials, Microstructure, Hysteresis, Polarization, PZT ceramics.

Resumen: Se realizaron análisis microestructurales y ferroeléctricos en cerámicas de $Pb_{1-3x/2}La_x(Zr_{0.54}Ti_{0.46})_{1-5y/4}Nb_yO_3$, x = y = 0.004, 0.006, 0.008 y 0.01% en moles. Se

utilizó microscopía de fuerza de respuesta piezoeléctrica (PFM) y lazo de histéresis piezoeléctrica (HL), se determinó el comportamiento ferroeléctrico y el tamaño de dominio ferroeléctrico. El tamaño de grano (determinado por SEM) y el área del dominio ferroeléctrico disminuyen con el aumento de la concentración del dopante de 3 µm a 1 µm y de 0,56 µm² a 0,32 µm², respectivamente. La máxima polarización remanente se obtuvo para $Pb_{1-3x/2}La_x(Zr_{0.54}Ti_{0.46})_{1-5y/4}Nb_yO_3$, lo que demuestra que las muestras se polarizan más fácilmente con una mayor concentración de dopante La^{3+} y Nb^{5+}. El campo coercitivo no presenta diferencias significativas ya que el contenido de La y Nb es variado. Los granos tienden a ser monocristales a medida que aumenta la concentración de los dopantes La^{3+} Nb^{5+}.

Keywords: Ferroelectric materials, Microstructure, Hysteresis, Polarization, PZT ceramics.

Introduction

The phenomenon of coupling between electrical and mechanical properties is a near-universal feature of inorganic, organic, and biological systems. The simplest example of linear electromechanical coupling is piezoelectricity, in which application of stress results in an electrical polarization (direct piezoelectric effect); while a mechanical displacement is produced by the application an electric field (converse piezoelectric effect). Since the discovery of piezoelectricity, at the end of the 19th century, piezoelectricity in inorganic materials has been studied in great detail, an achievement that was made possible by the combination of macroscopic measurements which provided information about properties and of atomic structure elucidated by advanced diffraction theories (Lines et al 1977). From symmetry considerations, piezoelectricity can exist only in non-symmetric polar materials (Nye 2001).

Complex examples of electromechanically active materials are ferroelectrics, in which polarization and hence directionality of electromechanical activity can be switched by external electric (ferroelectric) or mechanical (ferroelastic) stimuli. After the discovery of piezoelectricity in ferroelectrics, numerous applications such as sensors, actuators, transducers, etc. have emerged (Hench et al. 1990, Setter et al. 1993). In the last decade, the developments of deposition techniques for epitaxial ferroelectric thin films and advanced ceramic fabrication have resulted in numerous novel applications such as those in micro and nano-electromechanical systems (MEMS) (Polla et al. 1998, Dabbs et al. 2000, Schonholzer et al. 1999). The

ability of ferroelectric materials to exist in two or more polarized states, to conserve their polarization for a finite period, and to change the polarization under an electric field allows their consideration for non-volatile computer memory devices (FRAM) (Palkar et al. 1999, Suzuki 1995, Scott 2000).

In the last decade, piezoresponse force microscopy has become established as a powerful instrument for probing local electromechanical activity on the micro and nanometer scale (Jesse et al. 2006, Alexe et al. 2004, Hong 2004). Originally developed for imaging domain structures in ferroelectric materials, PFM was later extended to local hysteresis loops by piezoresponse force spectroscopy (Roelofs et al. 2000), as well as to ferroelectric domain patterning for applications such as high-density data storage (Tybell et al. 2002) and ferroelectric lithography (Kalinin et al. 2004, Terabe et al. 2003). It was suggested recently that the PFM vector could be used to determine local molecular or crystallographic orientation in piezoelectric materials, if all three components of the electromechanical response vector are determined quantitatively (Kalinin et al. 2006 a). Broad applicability of PFM to materials such as ferroelectric perovskite (Rodriguez et al. 2004), piezoelectric III–V nitrides (Rodriguez et al. 2002), and recently, biological systems such as calcified and connective tissues (Halperin

et al. 2004, Kalinin et al. 2005 and 2006 b), has required of fundamental theoretical studies of the image formation mechanism in PFM.

In this work, we study the relationship among structure (by X-ray diffraction, XRD)- and domain size by piezoresponse force microscopy (PFM), as well as polarization by hysteresis loops.

Materials and methods

Ceramics samples were prepare by solid-state reaction to obtain the following stoichiometric relationship $Pb_{1-3x/2}La_x(Zr_{0.54}Ti_{0.46})_{1-5y/4}Nb_yO_3$, where x = y = 0.004, 0.006, 0.008 and 0.010 mole % (abbreviated as PLZTN 54/46/0.4 for example). Mixture of the components is accomplished via humid milling with ethylic alcohol in an agate mortar mill during 90 minutes, and calcined at 960°C during 90 minutes in a covered alumina crucible. The samples pressed into pellets and sintered in lead atmosphere at 1250°C for 100 minutes. For ferroelectric characterization, some samples were metalized using silver paste.

The crystalline structure of the samples was analysed using a Rigaku DMax-2100 diffractometer with CuKα radiation (λ = 1.5418 Å) in the 2θ range from 15° to 60°. The crystalline size was calculated using the Scherrer formula (Cullity and Stock, 2001):

$$t = \frac{0.9\lambda}{B \cos \theta_B} \quad (1)$$

Where B is the full width at half maximum (FWHM) for the main peaks, t is diameter of the crystallite and θ_B is the Bragg angle selected.

Scanning Electron Microscopy (SEM) was carried out on fragmented samples in a microscope Philips model ESEMXL30 working at 15 kV and 16 mA, the magnification were 10 000 X.

Morphology, amplitude and phase images of samples were obtained in a Piezoresponse Force Microscopy (PFM); the measurements were performed working in the contact resonance tracking mode using a commercial DI-Veeco-Bruker Dimension 3100 Nanoscope IV AFM system, the signal from the photo detector position of the AFM was feed to a high frequency lock-in amplifier Stanford Research System SR844, where the signal was registered in amplitude an phase at the resonance frequency. Budget Sensors conductive probes were used, and DAQ NI-PCI-6133 card of national instruments was used for data acquisition. More details about the experimental technique were reported by Enriquez-Flores et al. 2012.

The hysteresis loops were obtained using a Radiant Technologies, Inc. and Trek High Voltage amplifier Model 609E-6 (Rivero et al. 2008). From which the ferroelectric characteristics of the materials were obtained: maximum applied electric field (EM), coercive field (EC), maximum polarization reached (PM) and remanent polarization (Pr).

Results and Discussion

Structure and morphology

The XRD patterns of the crystalline PLZTN powder show mixing of tetragonal and rhombohedral PZT phases (Fig. 1), characteristic of materials near to the morphotropic phase boundary (MPB) (Jaffe et al. 1971, Noheda et al. 2001).

For the lower lanthanum concentration, the relation between tetragonal and rhombohedral phases was approximately 57% tetragonal and 43% rhombohedral, for further lanthanum concentrations the presence of the tetragonal phase is increased like 66% -34% tetragonal - rhombohedral, respectively (Table I). On the other hand, the lattice constants are barely influenced by the dopant concentration (Suárez-Gómez et al. 2009, Durruthy-Rodríguez et al. 2010 and 2011). To quantify the phases concentration it was carried out the deconvolution of the (002)T, (200)T and (020)R picks and the areas of each phase was quantified (details in Fig. 1).
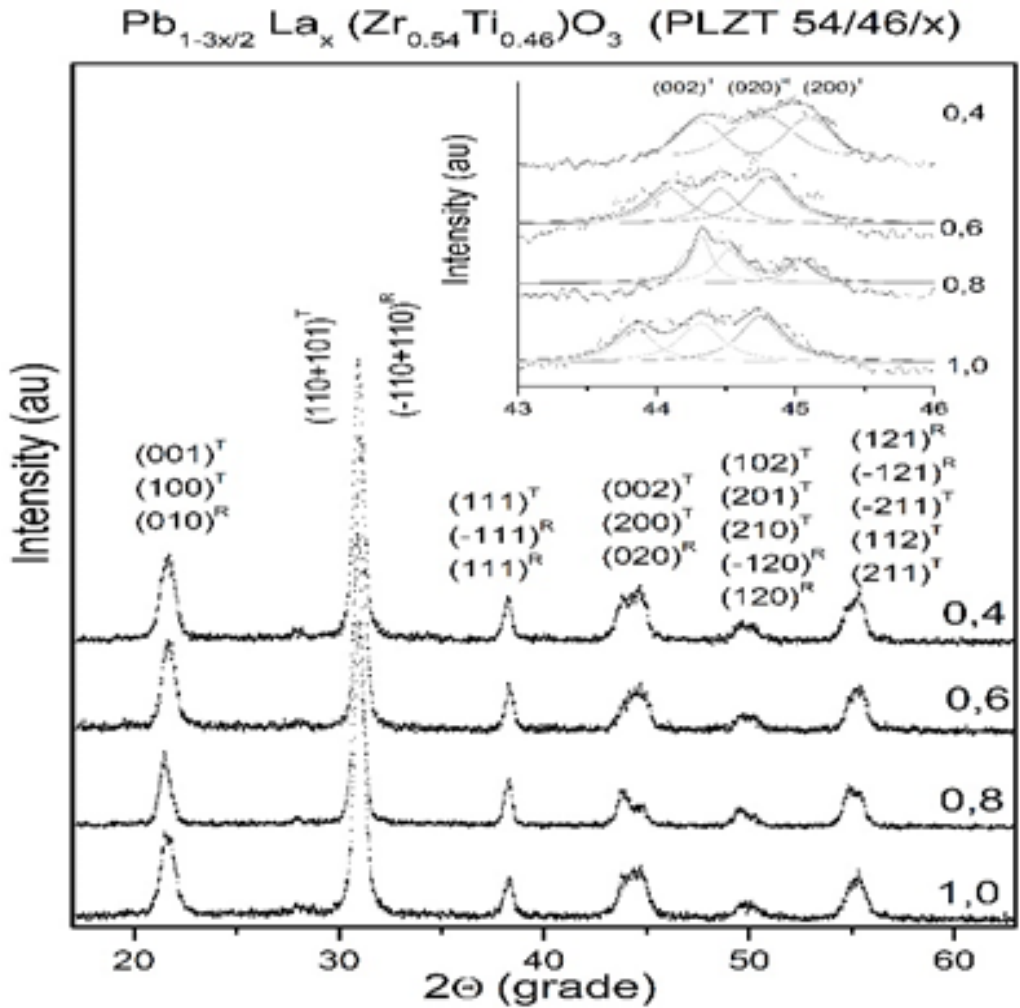
Figure. 1. Room temperature XRD patterns for Pb1-3x/2Lax(Zr0.54Ti0.46)1-yNyO3 sintered ceramics. In the detail appears like the peaks (200), (002) and (020) evolve with the dopant concentration for the phases tetragonal and rhombohedral, respectively.

The c/a ratio diminishes as the dopant concentration increases up to 0.008. In a previous work, it was found that by doping PZT ceramics with niobium or lanthanum separately does not influence the c/a ratio (Durruthy-Rodríguez et al. 2011) but, by using both dopants simultaneously there is a clear influence on this aspect.

The Fig. 2 shows the dependence of grain size with the both dopant concentration, with the increment of dopant concentration it diminishes strongly the grain size.

Table 1 shows that crystallite size and average grain size (σ grain size) depend directly and inversely with dopant concentration. In others words, crystallite number per grain size diminishes as the dopant concentration increase. The grain tendency is to formed single crystals.

Table 1. Parameters, ratio c/a, crystallite size and crystalline phase % for Pb1-3x/2Lax(Zr0.54Ti0.46)1-yNbyO3 samples.

% mol Dopant	Crystalline Phase %		Experimental Parameter			
	T	R	aR (Ao)	aT (Ao)	cT (Ao)	c/a
0.4	57	43	4,082 α=89,365	4,146	3,952	1,049
0.6	74	26	4,072 α=89,091	4,130	3,960	1,043
0.8	63	37	4,108 α=90,051	4,143	4,003	1,035
1.0	66	34	4,084 α=89,262	4,152	4,003	1,037
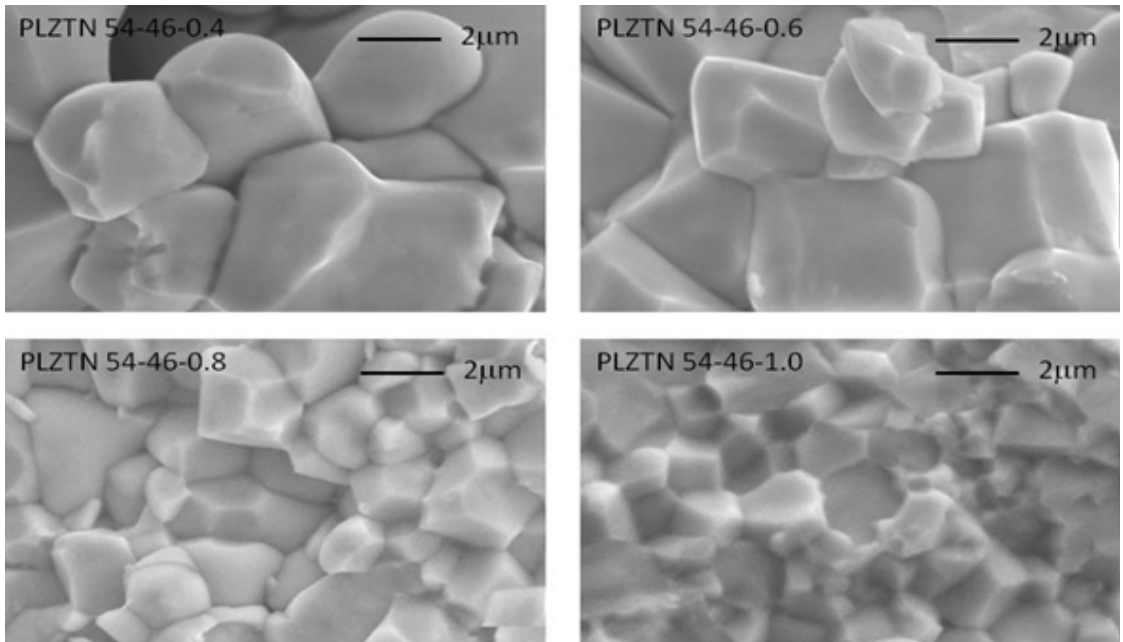
Figure. 2. SEM micrographs of fractured samples sintered at 1250ºC with dopant concentration of 0.4, 0.6, 0.8 and 1.0 % molar concentration. The grain size clearly diminishes with increasing dopant concentration.

Images of topography, amplitude, and phase, obtained in piezoresponse force microscopy (PFM) appear in Fig. 3a-l, for PLZTN 54/46/0.4, PLZTN 54/46/0.6, PLZTN 54/46/0.8 and PLZTN 54/46/1.0, respectively. The images show that the grain size diminishes as the dopant concentration increases from around 3 μm for PLZT 54/46/0.4 up to 1.0 μm for PLZT 54/46/1.0. Ferroelectric domain size also diminishes with the increase of the dopant concentration from 0.56 μm2

to 0.32 μm2. In a PFM amplitude image shows the borders of the domains walls, phase shows the extension of the domains and the contrast indicates the orientation of the domain "↑" or "↓" (Soergel 2011). Fig. 3 shows the image of a grain in topography as shown in the same amplitude and phase change color indicating the difference in the polarization direction. The measurements are performed in each case at the local resonance frequency (its value is shown in the figures).
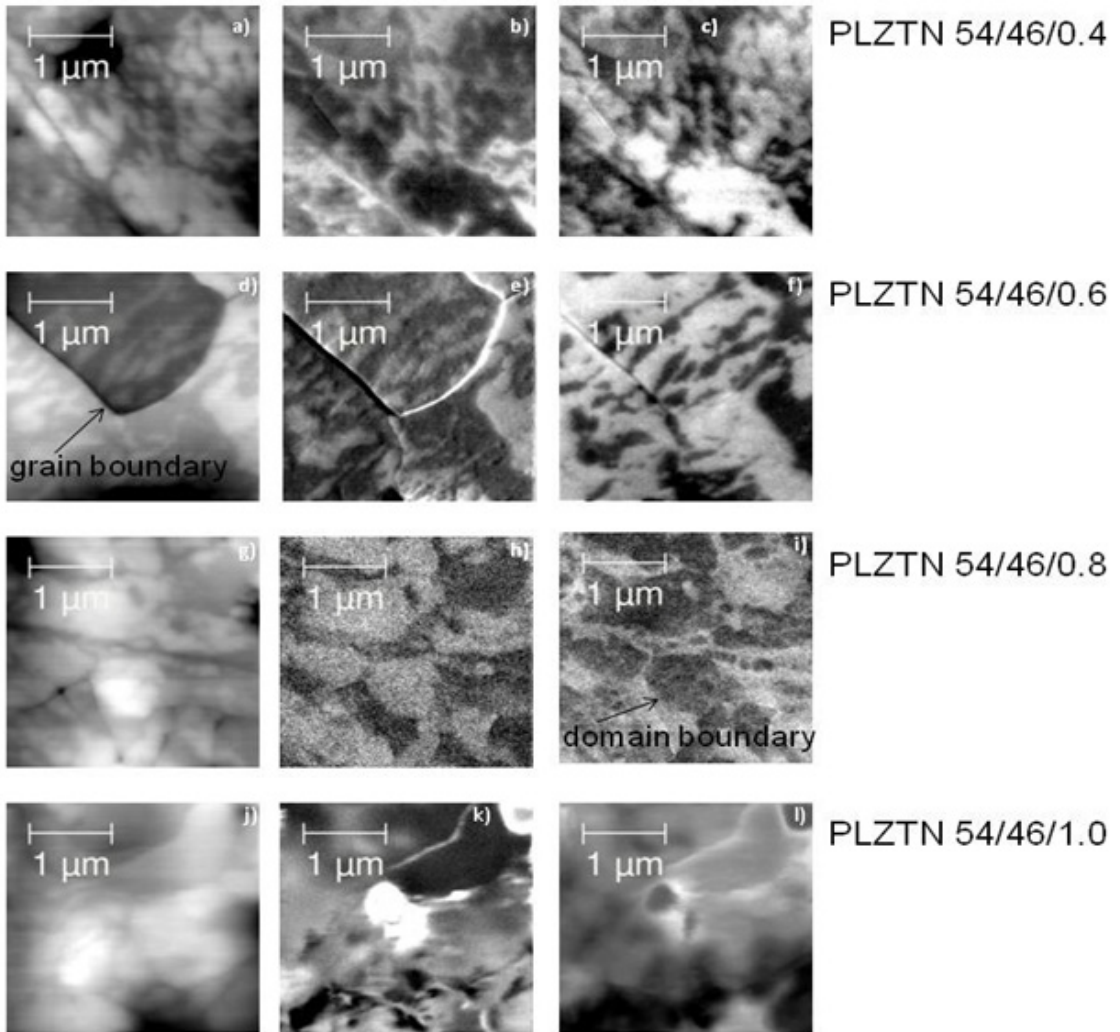
Figure. 3. Images of topography (a), d), g), and j)), PFM amplitude (b), e), h), and k)) and PFM phase (c), f), i), and l)) of PLZTN x/54/46/x samples with x = 0.4, 0.6, 0.8 and 1.0, respectively.

On the other hand, the tetragonal and rhombohedral crystallite area and grain area were calculated in order to compare it with ferroelectric domain area. For tetragonal crystallite size we take the sizes of crystallite size for (002) and (200) planes and then multiply them together; for rhombohedral crystallite size area, we take the crystallite size for (020) squared and divided by 2. For grain area, we assumed

grains are spherical; therefore we have used the expression πr^2, where r is the statistic half size (σ Grain size) reported in Table I. As was shown in Fig. 3, for PLZT 54/46/0.4 and PLZT 54/46/0.6 the approach used is not the same from the real morphology.

The area of the crystallite size grows with increasing dopant concentration, the relationship between crystallite size area and grain size area (AC-G) increases with dopant concentration increases, this contributes to form grains that will be considered as mono-domains (Fig. 4), the ratio AC-G varies for tetragonal and rhombohedral phase from approximately 0.002 to 0.008 and from 0.0003 to 0.001, when the dopant concentration varies from x=y=0.4 to 1.0 respectively (Table II). Similarly, the relationship among ferroelectric domain areas and grain area (ADF-G) it grows with the increment of dopant concentration (Table II).

The results of the polarization of a material among other aspects are influenced by microstructural aspects, crystallographic phase, the grain size and morphology of the ferroelectric domain.

Table 2. Evolution of crystallite, grain size, ferroelectric domain area and the relationship between there AC-G and ADF-G of PLZTN 54/46/x ceramics sintered.

La-Nb dopant concentration	Tetragonal crystallite size area (nm2)	Rhombohedral crystallite size area (nm2)	Grain size area (µm2)	AC-G x10-3	ADF-G
0,4	48.97	8.84	25.64	0.002 (T) 0.0003 (R)	0.022
0,6	62.98	9.58	21.50	0.003 (T) 0.0004 (R)	-
0,8	67.28	10.92	9.82	0.007 (T) 0.001 (R)	-
1,0	72.54	11.11	9.05	0.008 (T) 0.001 (R)	0.035

Table 3. Ferroelectric characteristics of the samples derived from the hysteresis loops.

La-Nb dopant concentration	EC (kV/cm)	EM (kV/cm)	Pr (µC/cm2)	PM (µC/cm2)	EC/EM	Pr/PM
0.4	3248	8846	15.17	20.56	0.37	0.74
0.6	3617	9374	8.26	12.72	0.39	0.65
0.8	2980	6622	14.92	19.95	0.45	0.75
1.0	3342	8221	23.84	30.68	0.41	0.78

PLZTN 54/46/0.4 **PLZTN 54/46/1.0**

$A_{C-G} = \begin{array}{l} 0.002\ (T) \\ 0.0003\ (R) \end{array}$ $A_{C-G} = \begin{array}{l} 0.008\ (T) \\ 0.001\ (R) \end{array}$
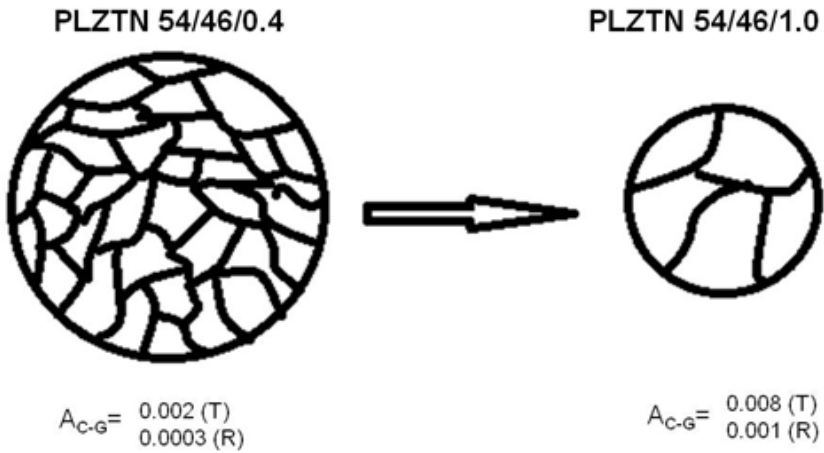
Figure. 4. Relationship between crystallite size area and grain area (AC-G).

The presented results show that as consequence of having a more rhombohedral phase concentration (this phase contributes with eight direction of polarization) and the increase of the domain sizes, the maximum of polarization remainder is obtained in the PLZTN 54/46/1.0 samples (Figure 5).
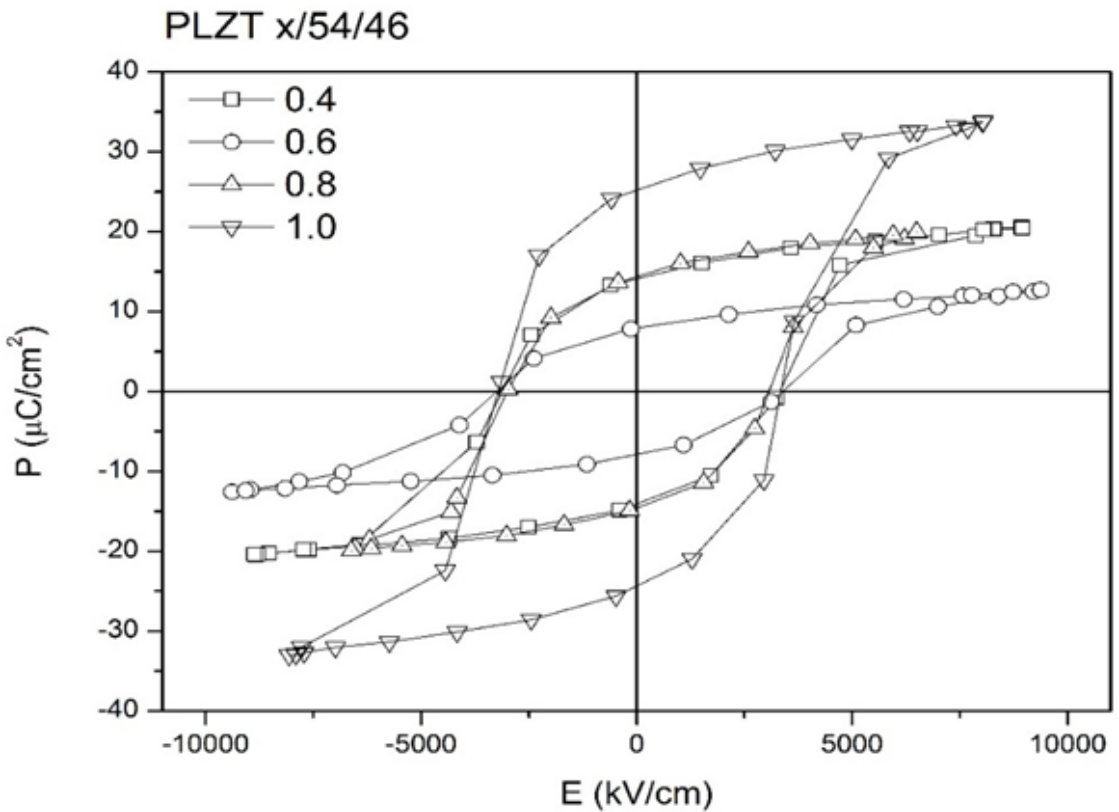
Figure. 5. Hysteresis loop for PLZTN 54/46/x

Ferroelectric hysteresis loop showed that the coercive field (Ec) (Table III) does not depend on the dopant concentration; this has been directly related with the average grain size (σ Grain size) these materials have the same order in size (Table I). However, the remanent polarization (Pr) was influenced very much by the increment of the dopant (Zhu et al. 2012). The polarization values obtained are acceptable for these materials (Table III).

Conclusions

In our days, the art of getting good ferroelectric materials is not a simple summation of properties. If we relate nanoscopic, microscopic and macroscopic aspects are not simply selecting the maximums for each case. Thus in ferroelectric PZT double substitution at A and B sites for La3+ and Nb5+, respectively, the materials with higher macroscopic polarization are those with smaller grain size, an appropriate mixture composition of the tetragonal and rhombohedral phases, with crystal size for each phase close to each other, which promotes the macroscopic polarization of the obtained ceramics.

On the other hand, the lattice constant is lightly influenced by the dopant concentration. The grain size and ferroelectric domain size diminish with the increment of dopant concentration but the crystallite size remains almost constant.

References

Alexe M., Gruverman A. 2004. Nanoscale Characterization of Ferroelectric Materials. Berlin. Springer. 279 p.

Cullity B.D., Stock S.R. 2001. Elements of X-Ray Diffraction. Third ed. New Jersey-Uppper Saddle River. Prentice Hall. 664 p.

Dabbs D.M., Aksay I.A. 2000. Self-assembled ceramics produced by complex-fluid templation. Annu. Rev. Phys. Chem. 51, 601-22.

Durruthy-Rodríguez M. D., Costa-Marrero J., Hernández-García M., Calderón-Piñar F., Yañez-Limón J. M. 2010. Photoluminescence in ¨hard¨ and ¨soft¨ ferroelectric ceramics. Applied Physics A: Materials Science & Processing 98, 543-550.

Durruthy-Rodríguez M. D., Costa-Marrero J., Hernández-García M., Calderón-Piñar F., Malfatti C., Yáñez-Limón J. M. 2011. Optical characterization in Pb(Zr1-xTi x)1-y NbyO3 ferroelectric ceramic system. Applied Physics A: Materials Science & Processing 103, 467-476.

Enriquez-Flores C.I., Gervacio-Arciniega J.J., Cruz-Valeriano E.; de Urquijo-Ventura P., Gutierrez-Salazar B.J., Espinoza-Beltran F.J. 2012. Fast frequency sweeping in resonance-tracking SPM for high-resolution AFAM and PFM imaging. Nanotechnology 23, 495705.

Halperin C., Mutchnik S., Agronin A., Molotskii M., Urenski P., Salai M., Rosenman G. 2004. Piezoelectric effect in human bones studied in nanometer scale. Nano Lett. 4, 1253-1256.

Hench L.L., West J.K. 1990. Principles of Electronic Ceramics. New York. Wiley. 576 p.

Hong S. 2004. Nanoscale Phenomena in Ferroelectric Thin Films. Dordrecht. Kluwer. 277 p.

Jaffe B., Cook W.R., Jaffe H. 1971. Piezoelectric Ceramics. London-New York. Academic Press. 328 p.

Jesse S., Baddorf A.P., Kalinin S.V. 2006. Dynamic behaviour in piezoresponse force microscopy. Nanotechnology 17, 1615-1628.

Kalinin S.V., Bonnell D.A., Alvarez T., Lei X., Hu Z., Shao R., Ferris J.H. 2004. Ferroelectric Lithography of Multicomponent Nanostructure. Adv. Mat. 16, 795-99.

Kalinin S.V., Rodriguez B.J., Jesse S., Shin J., Baddorf A.P., Gupta P., Jain H., Williams D.B., Gruverman A. 2006 a). Vector piezoresponse force microscopy. Microsc. Microanal. 12, 206-20.

Kalinin S.V., Rodriguez B.J., Jesse S., Thundat T., Grichko V., Baddorf A.P., Gruverman A. 2006b). Bioelectromechanical imaging by scanning probe microscopy: Galvani's experiment at the nanoscale. Ultramicroscopy 106, 334-40.

Kalinin S.V., Rodriguez B.J., Jesse S., Thundat T., Gruverman A. 2005. Electromechanical imaging of biological systems with sub-10 nm resolution. Appl. Phys. Lett. 87, 053901-11.

Lines M.E., Glass A.M. 1977. Principles and Applications of Ferroelectric and Related Materials. Oxford. Clarendon Press; 680 p.

Noheda B., Cox D.E., Shirane G., Guo R., Jones B., Cross L.E. 2001. Stability of the monoclinic phase in the ferroelectric perovskite PbZr1-xTixO3. Phys. Rev. B 63, 14103.

Nye J.F. 2001. Physical Properties of Crystal. Oxford. Clarendon Press. 324 p.

Palkar V.R., Purandare S.C., Pinto R. 1999.

Ferroelectric thin films of PbTiO3 on silicon. J. Phys. D 32, R1-R18.

Polla D.L., Francis L.F. 1998. Processing and Characterization of piezoelectric materials and integration into microelectromechanical systems. Annu. Rev. Mater. Sci. 28, 563-97.

Rivero D., Portelles J., Benavides J.I., Hernández M., Quiles F.J., Díaz M. 2008. Semiautomatic installation to measure the hysteresis knot in ferroelectric materials. Revista Cubana de Física 25B, 133-35.

Rodriguez B.J., Gruverman A., Kingon A.I., Nemanich R.J., Ambacher O. 2002. Piezoresponse force microscopy for polarity imaging of GaN. Appl. Phys. Lett. 80, 4166-68.

Rodriguez B.J., Gruverman A., Kingon A.I., Nemanich R.J., Cross J.S. 2004. Three-dimensional high-resolution reconstruction of polarization in ferroelectric capacitors by piezoresponse force microscopy. J. Appl. Phys. 95, 1958-1962.

Roelofs A., Boettger U., Waser R., Schlaphof F., Trogisch S., Eng L.M. 2000. Differentiating 180o and 90o switching of ferroelectric domains with three-dimensional piezoresponse force microscopy. Appl. Phys. Lett. 77, 3444-3446.

Schonholzer U.P., Gauckler L.J. 1999. Ceramic Parts Patterned in the Micrometer Range. Adv. Mat. 11, 630-632.

Scott J. 2000. Ferroelectric Memories, Berlin: Springer Verlag. 120 p.

Setter N., Colla E.L. 1993. Ferroelectric Ceramics. Basel. Birkhauser Verlag. 161 p. Soergel E. 2011. Piezoresponse force microscopy (PFM). J. Phys. D: Appl. Phys. 44, 464003-20.

Suárez-Gómez A., Durruthy M.D., Costa-Marrero J., Peláiz-Barranco A., Calderón-Piñar F., Saniger-Blesa J.M., de Frutos J. 2009. Properties of the PLZTN x/54/46 (0.4 ≤ x ≤ 1.4) ceramic system. Materials Research Bulletin 44, 1116–1121.

Suzuki M. 1995. Review on future ferroelectric nonvolatile memory: FeRAM. J. Ceram. Soc. Jpn. 103, 1099-1111.

Terabe K., Nakamura M., Takekawa S., Kitamura K., Higuchi S., Gotoh Y., Cho Y. 2003. Microscale to nanoscale ferroelectric domain and surface engineering of a near-stoichiometric LiNbO3 crystal. Appl. Phys. Lett. 82, 433-35.

Tybell T., Paruch P., Giamarchi T., Triscone J.M. 2002. Domain Wall Creep in Epitaxial Ferroelectric Pb(Zr0.2Ti0.8)O3 Thin Films. Phys. Rev. Lett. 89, 097601-1-4.

Zhu W., Fujii I., Ren W., Trolier-McKinstry S. 2012. Domain Wall Motion in A and B Site Donor-Doped Pb(Zr0.52Ti0.48)O3 Films. J. Am. Ceram. Soc. 95, 2906-2913.